Atomic-resolution quantitative composition analysis using scanning transmission electron microscopy Z-contrast experiments

E. Carlino* and V. Grillo
Laboratorio Nazionale TASC-INFM, Area Science Park, S. S. 14, Km 163.5, 34012 Trieste, Italy

(Received 2 December 2004; published 3 June 2005)

Here a general approach to measure quantitatively with atomic resolution the distribution of a chemical species in a host matrix is derived and applied to a case study consisting of a layer of Si buried in a GaAs matrix. Simulations and experiments performed on Si/GaAs superlattices demonstrate a quasilinear dependence of the high-angle annular dark-field image intensity on the concentration of Si in the GaAs matrix. The results have been compared with those obtained by cross-sectional scanning tunneling microscopy on the same specimens.

DOI: 10.1103/PhysRevB.71.235303 PACS number(s): 68.37.Lp, 68.37.Ef, 68.65.Ac

I. INTRODUCTION

Current efforts to develop nanostructured materials and devices are stimulating the implementation of experimental probes of the structure and chemical composition of solids on the atomic scale. Over the years, transmission electron microscopy (TEM) has widely demonstrated its potential to study material structures with the highest spatial resolution available. More recently, the combination of scanning tunneling microscopy (STM) and high-angle annular dark-field imaging (HAADF) has shown promise as an analytical tool that can provide "chemical" information at atomic resolution.[1]

One of the strong advantages of HAADF relative to other TEM imaging techniques, such as phase-contrast high-resolution TEM (HRTEM), is related to the mainly incoherent nature of the image obtained by HAADF. As a result, HAADF images provide unambiguous information on the position of the atomic columns in a solid with subangstrom resolution. In 2002 a resolution of 0.07 nm was demonstrated in a HAADF image obtained using a scanning TEM (STEM) instrument equipped with spherical aberration coefficient correctors.[2] More recently, direct evidence of a resolution of 0.078 nm has been achieved allowing to distinguish the (444) atomic spacing in Si.[3] Furthermore, contrast in the HAADF image is approximately proportional to the square of the atomic number of the atomic species contained in the column and this is why this methodology is also known as Z-contrast imaging.[4] Hence, detailed chemical information can be directly obtained without the uncertainty related to the phase problem in HRTEM imaging.[5,6] One of the most important potential applications of high-resolution Z-contrast imaging[7–13] is related to sampling the concentration profile of a given chemical species in a host. It has been recently demonstrated that, by choosing the appropriate experimental conditions, HAADF imaging can be used to probe the Si distribution in GaAs with atomic resolution from the raw data, even without any image simulation.[1] Quantitative analysis requires further knowledge to extract the information on the atomic concentration from the experimental data. High-angle annular dark-field image intensity depends with a power law on the atomic number of the species contained in the specimen.[4] This exponent is slightly dependent on the atomic species considered and on the shape of the high-energy electron wave function within the specimen.[14] Here, a general method to calculate the HAADF image intensity for an alloy is derived and it is applied to measure quantitatively at atomic resolution the distribution of chemical species in a host matrix. Experiments performed on Si/GaAs (001) superlattices demonstrate a quasilinear dependence of the high-angle annular dark-field image intensity on the concentration of the Si in the GaAs matrix. Such test structures were selected because the expected Si distribution in Si δ-doped layers in GaAs and Si-GaAs superlattices is sharp enough to test the spatial resolution of our method and can be characterized, for comparison, also by cross-sectional scanning tunneling microscopy (XSTM).

II. EXPERIMENT

Samples on GaAs(001) wafers were grown by solid-source molecular beam epitaxy (MBE). A total of ten Si layers were fabricated at 580 °C interrupting the growth of the GaAs host crystal by closing the Ga shutter, opening the Si shutter, and leaving the As shutter open. Nominal Si layer thickness was 1 monolayer (ML), with 1 ML$=6\times10^{14}$ atoms cm^{-2}. The spacing between the Si layers was 50 nm. A 200-nm-thick *n*-GaAs layer was grown to cap the structure. The GaAs between the layers and up to 10 nm above and below the superlattice was undoped. The buffer layer below the stack and the cap layer above were *n*-doped (1.6×10^{17} Si donors cm^{-3}).

HAADF STEM experiments were performed on TEM specimens prepared in (110) cross-section geometry following a well-established procedure previously reported.[1] Special care was devoted to obtaining TEM specimens with clean and smooth free surfaces necessary for HAADF experiments. Just prior to inserting the specimen and the specimen holder in the TEM vacuum they were cleaned in high frequency low-energy plasma of argon and oxygen to remove the hydrocarbon contamination from the surfaces. TEM experiments were performed at room temperature using a Jeol 2010F UHR TEM/STEM electron microscope, with field-emission gun, operating at 200 kV (λ

 ©2005 The American Physical Society

=0.0025 nm), with a measured spherical aberration coefficient C_s of 0.47±0.01 mm and relevant interpretable resolution limit in phase contrast HRTEM of 0.19 nm.[15] The STEM attachment is equipped with a bright-field detector and a HAADF detector for high-resolution Z-contrast imaging. The theoretical resolution achievable in atomic resolution Z-contrast mode with the available electron optics is 0.126 nm (see below). Micrographs were acquired digitally in both phase contrast HRTEM and Z-contrast mode in STEM. Special care was used to measure the gain and the dark current of the HAADF detector because this step is necessary to quantify the analytical information contained in the contrast of the relevant images.

III. HAADF IMAGE FORMATION AND ITS DEPENDENCE ON THE SPECIMEN ATOMIC NUMBER

The crystal studied in atomic resolution transmission electron microscopy are considered to be oriented along well-defined directions in which the electron wave can propagate along well defined columns of atoms. In some cases, the features of the experimental image reproduce the position of the atomic columns in the crystal. This is the case when HAADF image are formed in the electron microscope. At the electron energies used in these experiments (of typically 200–300 keV) the scattering of an electron is not significantly dependent on the variation of the crystal potential in the direction along the columns and the wave function describing an electron in the crystal can be expressed in terms of the eigenstates of a two-dimensional form of the Schroedinger's equation.[16] The potential function is that for the projected structure in the plane perpendicular to the zone axis considered for the TEM/STEM experiment. In analogies with the eigenstates of atoms, the eigenstates for atomic columns have similar nomenclature s, p, d, etc. Some of the eigenstates have significant amplitude only close to the atomic column and can be expressed in terms of an eigenstate of an isolated column. An electron incident on the crystal usually excites several eigenstates. In the case of a small probe focused on an atomic column mainly the eigenstates peaked at the columns are excited. In particular, in this case, it is the lowest energy eigenstate 1s which determines the main feature of the wave emerging from the backface of the crystal and it is at the origin of the so-called s-state approximation used in the description of the features of HAADF image.[14,17] This approach shows its limit in cases when the atomic columns in the considered projection are spaced less than 0.09 nm or when the TEM/STEM specimen is so thick that the contribution of other Bloch states cannot be neglected.[17] The experiment performed in this work are realized to satisfy to large extent the 1s approximation. The 1s columnar Bloch states are ideal as object function if the aim is to solve the position of the atomic columns as they are the less dispersed around the positions of the atomic columns with a full width at half maximum (FWHM), for example, of only 0.06–0.08 nm in the case of GaAs.[18] The combined effect of the use of an annular STEM detector with a collection angle larger than 80 mrad and thermal diffuse scattering, relevant at high scattering angle,[19] produces an image in which the main contribution is given by the 1s columnar states.[20]

The intensity in a HAADF image is given by $I(r) = O(r)^* P^2(r)$, where $O(r)$ is the object function and $P^2(r)$ is the resolution function.[21] Hence, in an atomic resolution Z-contrast STEM experiment the resolution achievable is due to the size of the object function, $O(r)$, convoluted with the resolution function, $P^2(r)$, where the latter is the size of the electron beam scanned on the specimen.[22] The use of a field emission gun allows one to obtain small and highly coherent probes. The size of the smallest electron beam achievable in a STEM is given by 0.43 $C_s^{1/4}\lambda^{3/4}$,[23] where C_s is the spherical aberration coefficient of the objective lens and λ is the electron wavelength. Hence, in the present case, the used electron optical conditions give a probe size of 0.126 nm, well below the spacing of 0.28 nm of two consecutive GaAs dumbbells atoms in the (110) projection. Furthermore, the intensity in a HAADF image is strongly dependent on the atomic number of the chemical species in the atomic columns. In fact, the object function convoluted with the annular detector is given approximately by[24]

$$O(\mathbf{R}) = \beta^2 V^2(\mathbf{R}),$$

where β is the interaction constant m/h^2, m is the relativistic mass of the electron, and $V(\mathbf{R})$ is the projected potential.[25] Hence, for high scattering angles and thin specimens, the intensity of the spots in the images corresponds to the square of the projected crystal potential of the chemical species inside atomic column. Furthermore, in the 1s approximation the HAADF image intensity, as integrated on the whole large angle detector, is proportional to Z^2 where Z is the related to the atomic number of the atomic column. An accurate calculation of the Bloch states intensity in the framework of a purely dynamical theory shows that the quadratic dependence of Z is a good approximation,[14] even if, for quantitative results, the value of the exponent should be accurately calculated in order to avoid error in the measurement. Furthermore, a correction for the shape of the high-energy electron wave function in the specimen has to be applied. In fact, the cross section σ for each individual element of the atomic column is given by $\sigma = c(Z,\varepsilon) Z^{\alpha(Z)}$ where "c" is a coefficient of proportionality, Z is the atomic number, and ε is the energy of the primary electron beam. It is worthwhile to remark that, whenever the image intensity is used to derive the chemical content, the role of the strain on the image contrast has to be considered and, in particular, eventual artifacts related to the elastic relaxation occurring in the thin TEM specimen obtained from strained heterostructures.[26,27] In particular for the application shown in paragraph V a structure model consisting of a substrate of a pure (not alloyed) material and an epitaxial phase pseudomorphically grown is considered. As the epitaxial layer has a lattice parameter different from the substrate a complex distortion of its crystal cell occurs. As reported by Treacy *et al.*,[28] a collection angle higher than 80 mrad allows acquisition of mainly incoherent electrons in the HAADF image and, in our case, eliminates contributions to the image contrast due to strain at the Si-GaAs interface, where the high mismatch between the Si and

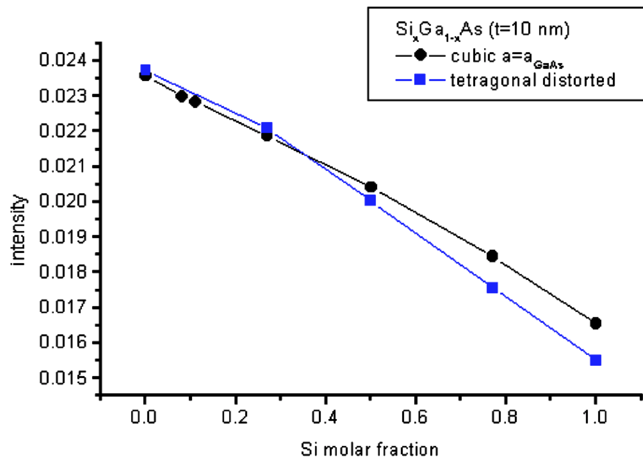

FIG. 1. (Color online) HAADF image intensity simulated in case of undistorted cell and in case of the tetragonal distortion produced by the lattice mismatch induced by the Ga(Si)As alloy on GaAs. The TEM specimen thickness is of 10 nm.

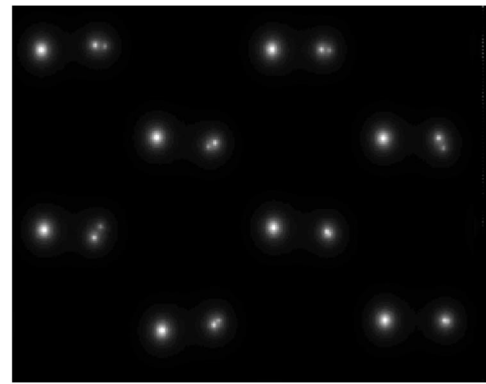

FIG. 2. Section of the potential grid used for simulating HAADF image in [110] zone axis of an alloy of Ga(Si)As. The appearance of doubling in the potential is due to the application of the frozen phonon approximation in presence of an alloy described by partial occupation procedure.

GaAs lattice parameters is expected to yield diffraction effects.[29] Nevertheless, for quantification, the lattice cell volume variation due to strain was considered in the simulation of the HAADF image intensities. Figure 1 shows the effect of the tetragonal distortion on the HAADF intensity. In the figure the intensity of the relevant HAADF images have been calculated as will be discussed in details below. As can be seen the tetragonal distortion can produce, in the worst case, an error in the intensity measurement of 6%.

Special care during implementation of the experimental setup has to be devoted to use of precise zone axis condition as a small tilt could produce a variation in the intensity of the image of the atomic column, even if do not change their positions in the HAADF image.[30] The use of the large angle convergent beam electron diffraction symmetries, as applied in this work, allows precise orientation of the crystal in the required zone axis.[31]

IV. HAADF IMAGE INTENSITY CALCULATION FOR RANDOM ALLOYS

To quantify the analytical content of a HAADF image it is necessary to simulate its intensities defining in a proper way the model structure.[32] As will be shown below, the HAADF image intensity calculation of an alloy depends on how the partial occupation of a species in the alloy is considered. The multislice approach is well known in the electron microscopy to be very versatile to handle complicated specimen structures.[33] In particular, the use of routines based on multislice method in the frozen phonon approximation has been recognized to give the most physical description of the electron probe-specimen interaction for HAADF experiments even if at the cost of very time-consuming calculations.[34] Here this approach will be used to calculate the HAADF image intensity as a function of the concentration of guest species in a host matrix.

In order to give a general account for the HAADF intensity dependence on single species molar fraction in an alloy two important points are to be clarified in this section regarding simulations and parametrization of simulation results.

First of all, it is necessary to clarify whether the so-called partial occupation procedure can be applied to HAADF simulations; the second point is related to the parametric expression describing the dependence of the intensity on molar fraction of species. The partial occupation concept is largely used in simulating an alloy in HRTEM images with reliable results.[35,36] In fact, in the simulation it is possible to account for a partial substitution of a species with another, as in a solid alloy, by simply considering a partial occupation coefficient x. This is also known in solid-state physics as "virtual crystal approximation."[37] The potential in each point becomes therefore simply a weighted linear combination of the potential of each species

$$V = x_1 V_1(\vec{r}) + x_2 V(\vec{r}) + \ldots = \sum_{i=\text{species}} x_i V_i(\vec{r}).$$

The virtual crystal approximation can be applied in this scheme for conventional simulation of HRTEM results and indeed it is largely applied producing reliable results.[15] The same kind of approach can yield formation of artefacts in simulated HAADF images due to the incoherent nature of the HAADF image. In fact, while the electron probe is propagating along the crystal column, it interacts with the potential of each atom and the results are influenced by the shape of such potential. To take into account the interaction with phonons along the direction of propagation, the atoms are displaced from their rest position and the final results are given by considering an appropriate configuration of atoms to reproduce the effect of the scattering with a phonon. This is at the origin of the so-called frozen-phonon approximation.[5] The approach works very well if in a certain position there is one atom but could fail if the position is occupied by x_A% of the potential of atom A and $(1-x_A)$% of the potential of atom B. In the random displacement of the two partial atoms the movement can be in the same direction or, more likely, in a different direction producing largely different results. Figure 2 shows the potential grid due to a

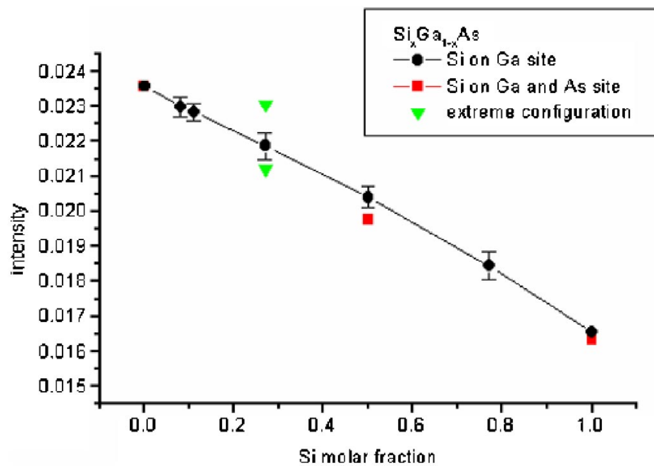

FIG. 3. (Color online) Intensity in the HAADF image as a function of the atomic arrangements in the column.

partial occupation of Si on Ga sites in GaAs projected along the [110] zone axis and used in the simulation performed by using a program based on the routines of Kirkland.[34] This routines fully accounts for the thermal diffuse scattering making use of the "frozen phonon" approximation. In this scheme the position of the atoms are randomly displaced from their rest position to account for thermal oscillation as described above. For each displacement configuration a conventional multislice calculation is performed. The doubling of several of the projected potential in Fig. 2 is an artifact due to considering the partial occupation in describing the alloy.

A possible solution to this inconvenient could be to displace both the weighted potentials in the same direction with a proper, not obvious, Debye-Waller factor or to consider the different configuration obtainable and to average on the all relevant results. This latter choice will be used here for the reason explained in the following. It is worthwhile to remark that this effect is not simply an error due to a wrong approximation, but depends on the incoherent nature of the HAADF image contrast formation. As a consequence, a dependence of the atoms configuration in the atomic column could produce different HAADF image intensity. In fact, if the *A*-*B* alloy is considered, within the limit of validity of the equation $I(r)=O(r)^{*}P^{2}(r)$, the incoherent contribution of a single atom in the column is weighted by the value of the resolution function P^2 at the atom position. Due to the channelling dynamical effects P^2, or better the density of the electron current in the specimen "J," shows a quite oscillating behavior. As a consequence, a different arrangement of the *A* and *B* atoms along a column could produce different intensity in the relevant HAADF image. This implies that no general statement can be made for a random alloy as long as the column configuration is not specified: this could produce a limitation in the direct interpretability of a column by column quantification in HAADF. For each column an error bar as large as the spread due to different configuration should be added. The quantitative evaluation of the effect of different configuration of the atoms in the column is reported in Fig. 3 where the results of simulations for a thickness of 10 nm in which different Si distributions are considered. The points indicate the case of random Si occupation of Ga sites, the squares indicate the case in which the same amount of Si is over both Ga and As sites, forming Si-Si complexes. It can be seen that the image intensity integrated over the total area of the cell is not so sensitive to the change of position of the silicon between the two columns in the dumbbell.

On the contrary, the in-depth configuration can potentially have a large effect, as demonstrated by the position of the triangles in Fig. 3: these indicate the result of simulation for the special configuration with all Si atoms (in this case 7) located at the beginning or the end of the atomic column.

The average of different configurations is expected to give more reliable results within the error bars reported in Fig. 3. This error bars is the standard deviation and represents in the worst case an error of about 2%. Furthermore, an average along the interface direction would further reduce the error on the experimental measurement. The analysis that follows will be therefore concentrated on the intensity deriving:

$$\tilde{I}=\frac{\sum_{i=\text{config}} I_i}{N_{\text{config}}}.$$

The second step to be considered is the interpolating expression to be used to derive the specimen composition from the intensity in HAADF. Considering an alloy of two species *A* and *B* with atomic number Z_A and Z_B and partial occupation x_A and x_B (the condition $x_A=1-x_B$ is considered) no fixed rule exists for the HAADF image intensity interpolation for the relevant alloys; nevertheless some power lawlike interpolation expressions can be attempted as[38]

$$I=m(Z_Ax_A+Z_Bx_B)^{\alpha} \tag{1a}$$

or

$$I=m_A(Z_Ax_A)^{\alpha}+m_B(Z_Bx_B)^{\alpha} \tag{1b}$$

or

$$I=m_Ax_A(Z_A)^{\alpha}+m_Bx_B(Z_B)^{\alpha} \tag{1c}$$

and in principle many other interpolation are possible, but actually some constrains exist. The natural requirement is that for $x_A=1$ ($x_B=0$) and $x_B=1$ ($x_A=0$) the correct dependencies Z^{α} are recovered. Furthermore, if $Z_A=Z_B$ the intensity must be independent of x. This is a natural requirement since for a fictitious substitution of a species with itself no change in intensity must appear. It is easy to see that, for example, Eq. (1b) does not fulfill this requirement while the other two do. As described above the intensity considered to calculate the HAADF image is given by

$$\tilde{I}=\frac{\sum_{i=\text{config}} I_i}{N_{\text{config}}}. \tag{2}$$

As $I=\int O(\bar{r},z)\otimes J(\bar{r}_p,z)dz$ and $O\approx\Sigma_{i=\text{atoms}}\sigma_i\delta(r-r_i,z-z_i)$,[39] it follows that:

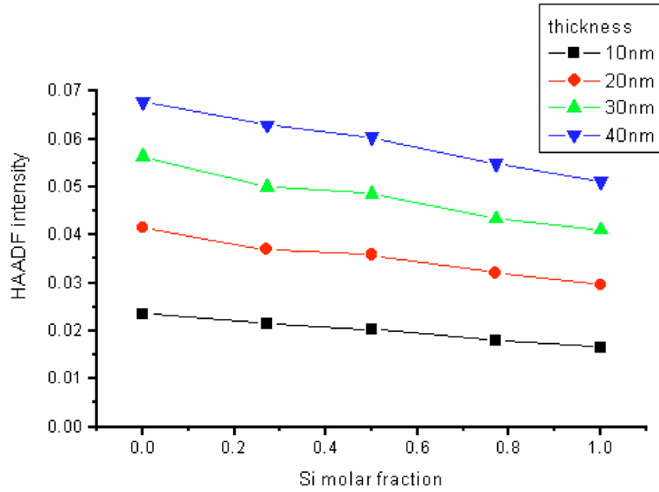

FIG. 4. (Color online) Intensity in the HAADF image as a function of the Si content and of the specimen thickness.

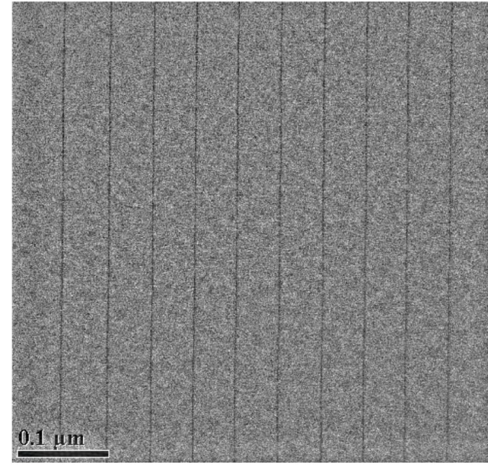

FIG. 5. Low magnification HAADF image of the Si/GaAs superlattice. The lower atomic number in the Si-rich region with respect to the GaAs gives rise to the ten sharp darker lines in the micrograph.

$$\tilde{I} = \frac{\sum_{i=\text{config}} I_i}{N_{\text{config}}} = \frac{\sum_{i=\text{config}} \left\{ \sum_{j=\text{atoms}A} [\sigma_A J_i(r_j,z_j)] + \sum_{j=\text{atoms}B} [\sigma_B J_i(r_j,z_j)] \right\}}{N_{\text{config}}} \tag{3}$$

the subscript "i" in J_i indicates that the current density within the specimen in general depends on the atomic configuration of the relevant column. In particular it can be assumed that J, for a given z coordinate, depends on the average composition before it. As a first approximation it will be assumed that 'J' is a function of the sole average composition x_A and x_B. This is an acceptable approximation, for what is discussed above, for quite uniform configurations while strong deviation are expected in the less likely configurations where atoms of the same kind are cumulating at one end of a column.

In this approximation the intensity can be rewritten using an average $J = J(r, z, \tilde{x}_A, \tilde{x}_B)$. If then the sum is transformed in a sum on atomic sites

$$\tilde{I} = \frac{\sum_{i=\text{config}} I_i}{N_{\text{config}}} = \sum_{j=\text{sites}} \left[\left(\frac{\sum_{i=\text{config}} x_{ijA}\sigma_A}{N_{\text{config}}} + \frac{\sum_{i=\text{config}} x_{ijB}\sigma_B}{N_{\text{config}}} \right) J(r_j, z_j, \tilde{x}_A, \tilde{x}_B) \right] = (\tilde{x}_A\sigma_A + \tilde{x}_B\sigma_B) \sum_{j=\text{sites}} [J(r_j, z_j, \tilde{x}_A, \tilde{x}_B)], \tag{4}$$

where the sites j has an occupancy x_{ijA} and x_{ijB} equal to 0 or 1 depending on which species is assumed to sit there in the ith configuration.

It is easy to see that, if the sum $\Sigma_{j=\text{sites}}[J(r_j, z_j, \tilde{x}_A, \tilde{x}_B)]$ were independent of x, a simple linear relationship could be used for extrapolating the intensity for an alloy. The dependence of P^2 on x, however, adds some degree of nonlinearity depending on the total specimen thickness. It should be a good parameterization therefore to write

$$\tilde{I} = (\tilde{x}_A\sigma_A + \tilde{x}_B\sigma_B) m(r_p, t, x_A, x_B) = m(r_p, t, x_A, x_B)(m_{0A}\tilde{x}_A Z_A{}^{\alpha_A} + m_{0B}\tilde{x}_B Z_B{}^{\alpha_B}). \tag{5}$$

Furthermore, if for example the intensity is not only considered on the maximum but it is averaged over a suitable area around the maximum for quantification then Eq. (5) can be further rewritten as

$$\tilde{I} = \left[\int m(r_p, t, x_A, x_B) dr_p \right] (\tilde{x}_A\sigma_A + \tilde{x}_B\sigma_B) = M(t, x_A, x_B)(\tilde{x}_A\sigma_A + \tilde{x}_B\sigma_B).$$

In fact, the simulation performed in the case of Si/GaAs in Fig. 1 or 3 shows how a quasilinear dependence of the HAADF image intensity on the Si content is obtained. This means that the dependence of $M(t, x_A, x_B)$ over x_A and x_B is small and in this case the contrast is independent on the TEM specimen thickness. This behavior is not true in general but should be considered case by case. Figure 4 shows the results of the simulations for a GaAs with partial substitution of Si on the Ga site. The intensity averaged in a unit cell is plotted against Si composition for different values of the thickness.

In the simulation the $Si_xGa_{1-x}As$ cell has been tetragonal distorted to satisfy the epitaxial match to GaAs. It is clear from Fig. 4 that for increasing thickness the intensity of both GaAs and SiAs extremes is increased and, hence, it can be defined the maximum contrast

$$C_{100\%} = \frac{I_{\text{GaAs}} - I_{\text{SiAs}}}{I_{\text{GaAs}}}.$$

$C_{100\%}$ is little varying with thickness as varies between 0.30 and 0.26 for increasing thickness from 10 to 40 nm. To a first approximation it can be assumed it is constant with an abso-

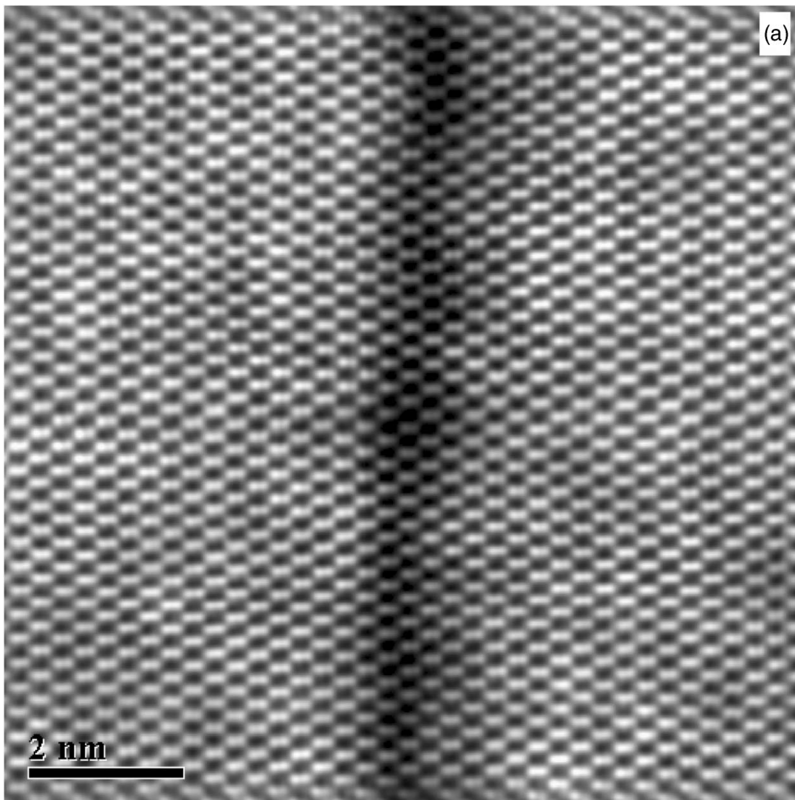

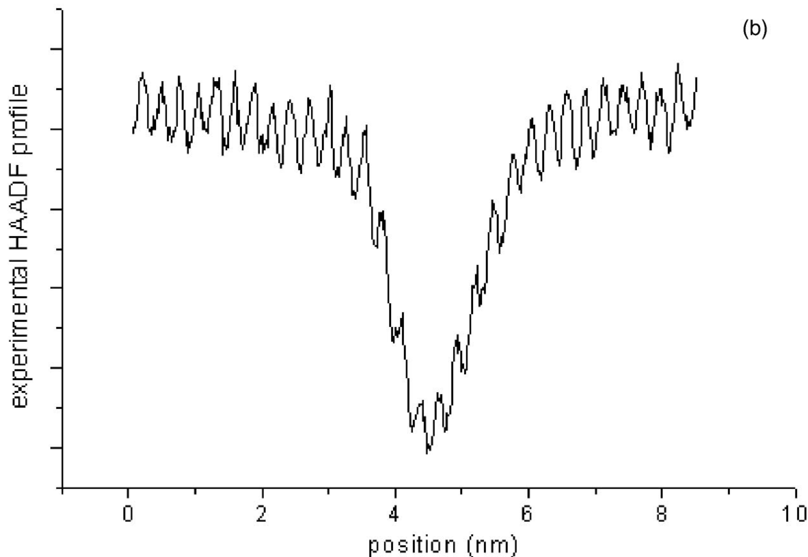

FIG. 6. (a) experimental HAADF image in [110] zone axis of one of the Si-rich region of Fig. 5. (b) Intensity profile across the Si rich region shown in (a).

lute error of about 0.02, namely $C_{100\%}=0.28\pm0.02$, this error can be larger for larger or lower thickness but it is a good reference as experimentally it is easy to perform an experiment for a thickness within the considered range. It is worthwhile to remark how the value of 28% is very close to the ratio of the cross sections $(\sigma_{\mathrm{GaAs}}-\sigma_{\mathrm{SiAs}})/\sigma_{\mathrm{GaAs}}=32\%$.

This assumption, however, permits to estimate the composition by simply using

$$x=\frac{C_{\mathrm{measured}}}{C_{100\%}},$$

where C_{measured} is the experimental contrast defined as $(I_{\mathrm{GaAs}}-I_{\mathrm{SiGaAs}})/I_{\mathrm{GaAs}}$.

V. MEASUREMENT OF Si PROFILE IN GaAs MATRIX

Figure 5 is a low magnification HAADF image in [110] zone axis of the epilayer. The collection angle was $84\leqslant 2\theta \leqslant 224$ mrad as in all the HAADF images here reported. Due to the lower atomic number of Si relative to GaAs, the ten Si layers give rise to the sharp dark lines spaced, as expected, by 50 nm of GaAs.

Figure 6(a) shows a high magnification atomic resolution HAADF image of one of the Si-rich layer. It is worthwhile noting how the image contrast, away from the Si-rich region, is homogeneous thus providing evidence for atomically flat specimen surfaces necessaries for a reliable contrast quanti-

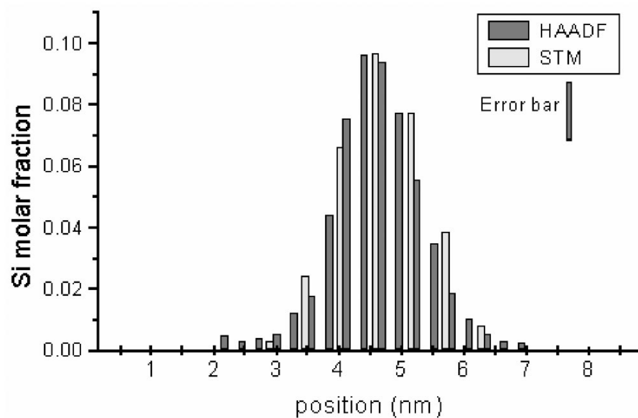

FIG. 7. Si composition profile in GaAs as measured by HAADF (dark-gray) and XSTM (light-gray). The number of dark-gray bars is double with respect the light-gray bars as resolution in the HAADF result is of 0.28 nm whereas in the XSTM the resolution is 0.56 nm. The error bar in the HAADF measurements is about 2%.

fication. A careful inspection of the elongated white dots in Fig. 6(a) allows one to distinguish the cation-anion columns seen projected onto the (110) plane and spaced by 0.14 nm. In Fig. 6(b) the experimental image intensity in Fig. 6(a) is plotted as a function of the distance from the interface. The higher peaks, 1.5 nm away from the minimum in the intensity profile, reflect the higher atomic number of the III–V species. The intensity decrease observed in going from the GaAs region toward the metallurgical Si-GaAs interface is due to the presence of Si in the atomic columns.

As the total area around the dumbbells is needed for comparison to simulations, the profile has been integrated obtaining a single point per dumbbell. In this averaging process we loose the initial resolution of Fig. 6(a). In fact, the distance between two consecutive peaks in Fig. 6(b) is 0.28 nm, in agreement with the expected cation or anion spacing in the bulk along the [001] direction. Hence, the detector background has been subtracted and the intensity value has been normalized to the GaAs regions on both sides of the dark Si-rich region. Applying the above-derived expression $x = C_{\text{measured}}/C_{100\%}$, the Si distribution was obtained and it is shown in Fig. 7 by the dark-gray bars. The Si distribution has been compared with the concentration obtained by XSTM and reported in Fig. 6 as light-gray bars. The methods used for the sample preparation, the image acquisition and the determination of the concentration profile from the XSTM data have been described in Refs. 1 and 40. The spacing between the XSTM data is twice that between the HAADF data because the spacing of the topmost Ga-As chains on the (110) surface, the atoms that can be sampled by XSTM, is 0.56 nm in the [001] direction.

VI. CONCLUSIONS

It has been shown how HAADF experiments can be used to measure at atomic resolution the chemical profile of a species in a host matrix. In order to establish a reliable quantification method some fundamental aspects of HAADF image formation of crystalline material have been investigated. The method has been applied to Si/GaAs superlattices demonstrating a quasilinear dependence of the high-angle annular dark-field image intensity on the concentration of Si in the GaAs matrix. Our results caution the readers about the artifacts that can be introduced in simulating HAADF results using virtual crystal approximation coupled with frozen phonon approximation. It has been measured the non-negligible influence of the atomic configuration within each atomic column on the relevant intensity of the HAADF image. This result marks how sensitive can be HAADF experiment in the study of special configuration as in the case of cluster formation. Furthermore, the sources of errors in the concentration measurement have been analyzed and their influence quantified together with the role of hydrostatic strain on HAADF image intensity.

As a result, the method allows us to quantify the Si content within the GaAs matrix with an error of ±2% demonstrating that Z-contrast imaging is an excellent tool to probe not only the structure but also the chemistry of solids at atomic resolution.

ACKNOWLEDGMENTS

The authors wish to warmly thank Alfonso Franciosi and Silvio Modesti for the useful discussions and suggestions.

*Electronic address: carlino@tasc.infm.it

[1] E. Carlino, S. Modesti, D. Furlanetto, M. Piccin, S. Rubini, and A. Franciosi, Appl. Phys. Lett. **83**, 662 (2003).
[2] P. E. Batson, N. Dellby, and O. L. Krivanek, Nature (London) **418**, 617 (2002).
[3] P. D. Nellist, M. F. Chisholm, N. Dellby, O. L. Krivanek, M. F. Murfitt, Z. S. Szilagyi, A. R. Lupini, A. Borisevich, W. H. Sides, Jr., and S. J. Pennycook, Science **305**, 1741 (2004).
[4] S. J. Pennycook and P. D. Nellist, *Impact of Electron Microscopy on Materials Research* (Kluwer Academic, Dordrecht, 1999), p. 161.
[5] S. J. Pennycook and D. E. Jesson, Phys. Rev. Lett. **64**, 938 (1990).
[6] P. D. Nellist and S. J. Pennycook, Ultramicroscopy **78**, 111 (1999).
[7] E. M. James and N. D. Browning, Ultramicroscopy **78**, 125 (1999).
[8] E. M. James, N. D. Browning, A. W. Nicholls, M. Kawasaki, Y. Xin, and S. Stemmer, J. Electron Microsc. **47**, 561 (1998).
[9] K. Mitsuishi, M. Kawasaki, M. Takeguchi, H. Yasuda, and K. Furuya, Ultramicroscopy **88**, 25 (2001).
[10] U. Kaiser, D. A. Muller, J. L. Grazul, A. Chuvulin, and M. Kawasaki, Nat. Mater. **1**, 102 (2002).
[11] P. M. Voyles, D. A. Muller, J. L. Grazul, P. H. Citrin, and H.-J. L.

Gossmann, Nature (London) **416**, 826 (2002).
[12] T. Yamazaki, K. Watanabe, Y. Kicuchi, M. Kawasaki, I. Hashimoto, and M. Shiojiri, Phys. Rev. B **61**, 13833 (2000).
[13] K. Watanabe, T. Yamazaki, Y. Kicuchi, Y. Kotaka, M. Kawasaki, I. Hashimoto, and M. Shiojiri, Phys. Rev. B **63**, 085316 (2001).
[14] S. J. Pennycook, *Advances in Imaging and Electron Physics* (Academic, New York, 2002), Vol. 123, p. 140.
[15] J. C. H. Spence, *Experimental High-Resolution Electron Microscopy*, 2nd ed. (Oxford University Press, New York, 1988).
[16] B. F. Buxton, J. E. Loveluck, and J. W. Steeds, Philos. Mag. A **38**, 259 (1978).
[17] G. R. Anstis, D. Q. Cai, and D. J. H. Cockayne, Ultramicroscopy **94**, 309 (2003).
[18] D. Van Dyck and M. Op de Beeck, Ultramicroscopy **64**, 99 (1996).
[19] C. Kittel, *Introduction to Solid State Physics*, 6th ed. (Wiley, New York, 1986), p. 602.
[20] B. F. Buxton, S. J. Loveluck, and J. W. Steeds, Philos. Mag. B **38**, 259 (1978).
[21] P. D. Nellist and S. J. Pennycook, J. Microsc. **190**, 159 (1998).
[22] S. J. Pennycook, *Advances in Imaging and Electron Physics* (Academic, New York, 2002), Vol. 123.
[23] O. Scherzer, J. Appl. Phys. **20**, 20 (1949).
[24] S. J. Pennycook, D. E. Jesson, P. D. Nellist, M. F. Chisholm, and N. D. Browning, *Handbook of Microscopy* (VCH, Weinheim, 1997), p. 595.
[25] P. Hirsh, A. Howie, R. B. Nicholson, D. W. Pashley, and M. J. Whelan, *Electron Microscopy of Thin Crystals*, 2nd ed. (Krieger, New York, 1977).
[26] L. De Caro, A. Giuffrida, E. Carlino, and L. Tapfer, Acta Crystallogr., Sect. A: Found. Crystallogr. **A53**, 168 (1997).
[27] S. Hillyard, Ultramicroscopy **58**, 6 (1995).
[28] M. M. J. Treacy, A. Howie, and S. J. Pennycook, Inst. Phys. Conf. Ser. **52**, 261 (1980).
[29] D. D. Perovic, C. J. Rossouw, and A. Howie, Ultramicroscopy **52**, 353 (1993).
[30] T. Yamazaki, M. Kawasaki, K. Watanabe, I. Hashimoto, and M. Shiojiri, Ultramicroscopy **92**, 181 (2002).
[31] J. W. Steeds and E. Carlino, in *Proceedings of the International School on Electron Microscopy in Materials Science*, edited by P. G. Merli and M. Vittori Antisari (World Scientific, Singapore, 1992), p. 279.
[32] G. R. Anstis, S. C. Anderson, C. R. Birkeland, and D. J. H. Cockayne, Scanning Microsc. Suppl. **11**, 287 (1997).
[33] P. Goodman and A. F. Moodie, Acta Crystallogr., Sect. A: Cryst. Phys., Diffr., Theor. Gen. Crystallogr. **A30**, 322 (1974).
[34] E. J. Kirkland, *Advanced Computing in Electron Microscopy* (Plenum, New York, 1998).
[35] P. A. Stadelmann, Ultramicroscopy **21**, 131 (1987).
[36] CERIUS Molecular Modeling Software for Material Research from Molecular Simulation Inc. of Burlington (MA) and Cambridge (UK).
[37] P. Y. Yu and M. Cardona, *Fundamentals of Semiconductors* (Springer-Verlag, Berlin, 1996), p. 182.
[38] T. Walther and C. J. Humphreys, J. Cryst. Growth **197**, 113 (1999).
[39] P. M. Voiles, Ultramicroscopy **96**, 251 (2003).
[40] S. Modesti, R. Duca, P. Finetti, G. Ceballos, M. Piccin, S. Rubini, and A. Franciosi, Phys. Rev. Lett. **92**, 086104 (2004).